Proceedings of the 9th International Symposium on
Dynamics and Control of Process Systems (DYCOPS 2010),
Leuven, Belgium, July 5-7, 2010
Mayuresh Kothare, Moses Tade, Alain Vande Wouwer, Ilse Smets (Eds.)

MoPostersT6.2

Multi-resolution Fuzzy Clustering Approach for Image-Based Particle Characterization

B. Zhang*, R. Mukherjee*, A. Abbas**, J.A. Romagnoli*,[1]

*Depart. Of Chemical Engineering, Louisiana State University, Baton Rouge, LA 70803,USA
** School of Chemical and Biomolecular Engineering, The University of Sydney, Sydney, NSW, 2006, Australia

Abstract: This paper presents a novel technique based on combing wavelet transform and Fuzzy C-means Clustering (FCM) for particle image analysis. Through performing wavelet transform on images, the noise and high frequency components of images can be eliminated and the textures and features can be obtained. FCM is then used to divide data into two clusters to separate touching objects. To quantitatively evaluate this method, a case study involving a particle image is investigated. The procedure of selecting optimum wavelet function and decomposition level for this image is presented. 'Fuzzy range' is used as a derived feature for segmentation. The amounts of particles, particle equivalent diameters, and size distribution before and after partition are discussed. The results show that this method is effective and reliable.

1. Introduction

Particulate processes are universal in pharmaceutical and fine chemical industries amongst others. Particle properties such as size and shape are related to operation conditions. The desired particle size distribution and shape can be obtained through adjustments of process conditions like flow, filtration, mixing and others at different stages of processing. However, the inevitable process disturbances during particle formation and production can affect its properties. Hence monitoring and controlling the particulate systems (suspensions, slurries, powders etc) are very important. Image analysis is a very promising method for direct measurements of particle size distribution and shape and it can be performed in real time. Accurately extracting quantitative information from particle images is necessary and important since whether to change operation conditions or not and the direction of changing depend on it.

Image segmentation is one of the most crucial and challenging tasks in image analysis. It is widely used in object detection (Korath et al., 2008; Sun et al., 2009). Since most image processing procedures come after the separation step, the eventual success or failure of image analysis largely relies on segmentation accuracy. The goal of segmentation is to divide the digital image into different visually distinct regions or objects. Many segmentation techniques have been developed and reported. Reviews of various segmentation techniques are given by Fu and Mui (1981), Pal and Pal (1993), and Cufi et al. (2002). However, no specific approach can be suitably applied to all the kinds of images and similarly, all the available separation algorithms may not perform successfully or efficiently on a particular image because the images come from different application fields and environments. For example, a segmentation technique used in images for remote control applications may not be suitable for medical images.

In this paper, a novel approach based on combing wavelet transform (multi-resolution) and Fuzzy C-means Clustering (FCM) for image segmentation is proposed. Wavelet transform has been widely used for multi-resolution analysis in the last two decades. Basically it is used for 1D signal (time series) processing. An image can be taken as a 2D signal where the temporal is replaced by spatial information. Wavelet transform makes it possible to investigate a signal (image) in both time (space) and frequency domain at the same time. In our research, wavelet transform is used to identify the image surface self without noise and high frequency components (Sun et al., 2008). Pattern recognition analysis, in terms of FCM is then incorporated for clustering analysis of the image at the surface self. With FCM method, we differentiated objects and background, identified the objects and boundaries and separated the touching areas. A new derived feature called 'fuzzy range' is incorporated to extract the touching area for segmentation. No neighborhood based calculation is needed when using fuzzy range other than traditional features like standard deviation or gradient.

2. Image Analysis by Wavelet Transform

Any image can be considered as a combination of the image self and imaging artifacts (noise). A recent computational technique, wavelet decomposition, can successfully separate the image underlying structure, in the form of the low frequency sub-image, image details, in the form of high frequency sub-images, as well as the imaging noise. High-frequency details and the imaging artifacts are difficult to differentiate, since they all fall into the high frequency range. The most convenient way to calculate different image characterizing features are also obtained from wavelet coefficients.

The images are represented by intensity of pixels in a 2D array. Since the data are discrete, a 2D discrete wavelet transformation is performed.

2.1. Discrete Wavelet Transformation

In a discrete wavelet transformation, discrete value of scale a and location parameter b are used (Addison P.S. 2002). They are discretized in such a manner that a and b are linked.

The scale a is generally discretized in a logarithmic way a_0^m where m is an integer. Each location b can be reached in discrete steps n (an integer) from an origin. It is also proportional to the scale a_0^m. Thus it can be represented as $nb_0a_0^m$. The wavelet function $\psi_{m,n}$ in the discrete form is

$$\psi_{m,n}(x) = \frac{1}{\sqrt{a_0^m}}\psi(a_0^{-m}x - nb_0) \qquad (1)$$

Where a_0 is a fixed dilation parameter and is greater than 1and b_0 is the location parameter and is greater than zero. The discrete wavelet transformation of function $f(x)$ is thus a function of m and n instead of a and b respectively.

$$T_{m,n} = \int_{-\infty}^{\infty} f(x)\psi_{m,n}(x)dx \qquad (2)$$

Discrete wavelet transformation $T_{m,n}$ is known as wavelet coefficient or detail coefficient. The most common way of discretization is to use a dyadic grid where a_0 and b_0 are 2 and 1 respectively. Discrete dyadic wavelets are orthonormal in nature. The original function can be reconstructed using the wavelet coefficients.

$$f(x) = \sum_{m=-\infty}^{\infty} \sum_{n=-\infty}^{\infty} T_{m,n}\psi_{m,n}(x) \qquad (3)$$

In moving from 1D to 2D wavelet transform, the rows and columns of the data matrix (x and y coordinates) that represent the image are treated as independent. Therefore, the 2D filters become the tensor products of their 1D counterpart. The scaling and wavelet functions for a 2D transform is obtained from tensor product of the one dimensional scaling and wavelet functions.

2.2 The Choice of Wavelet Function and Wavelet Decomposition Level

Since there are several wavelet functions available, the selection of optimal wavelet function, for the particular application, is the first problem to be tackled when applying the transform on an image. Wavelet functions are catalogued into various wavelet families and the most common ones are: Haar, Daubechies, Biorthogonal, Coiflets, Symelets. For some wavelet families, such as Daubechies, their member numbers are not constrained to only one. Different wavelet functions will generate different transforms, central frequencies and vanishing moments. By performing the transform using a wavelet function on a specific image, the decomposed sub-images will present the features in terms of frequency and spatial localization in response to the characteristics of the wavelet function. However, that wavelet function may or may not be able to capture the actual information from the image. Also an optimal function selected for one image may not be the best for another situation. The accuracy of image analysis results therefore depends on the selection of wavelet function.

Another issue that needs to be addressed is level of decomposition where we get the surface self without image artifacts. Theoretically, for an image whose pixel number is m in both directions, n decomposition levels can be performed if n satisfies the condition of $2^n \le m < 2^{n+1}$. As the image is decomposed to a certain level, the intrinsic information is totally smoothed out. However, the artifacts of the wavelet function will be added to the corresponding

approximation if the decomposition process continues. In order to maintain the true characteristics and also remove irrelevant noise and high frequency components of the image at the same time, it is necessary to find a suitable decomposition level.

Entropy measures can be employed to help identify the appropriate wavelet function and decomposition level which would yield an approximate sub-image with maximum information with respect to the key features for proper image segmentation. Among different entropy criteria, Shannon Entropy is applied. The concept of Shannon Entropy is sometimes referred to as a measure of uncertainty and is defined for a discrete probability distribution p_i:

$$S(p) = -\sum_{i=1}^{n} p_i \log(p_i)$$
$$where \ \sum_{i=1}^{n} p_i = 1 \qquad (4)$$

n is the total number of possible classes. The probability distribution is obtained from the normalized wavelet coefficient energies:

$$\bar{T}_{m,n}^2 = \frac{T_{m,n}^2}{\sum_{m=1}^{M} \sum_{n=1}^{N} T_{m,n}^2} \qquad (5)$$

The idea of Shannon Entropy as the criteria to identify the 'best' decomposition level is based on the measurement of the randomness for a given image. The more random parts existing, the more Shannon Entropy value the approximation image has. By performing the wavelet analysis on an image using a particular wavelet function, the Shannon Entropy will decrease at first due to the removal of noises and high frequency components. However, as the procedure goes on, it will increase after a certain level because of the added artifacts from the wavelet. So the decomposition level at which the first minimum Shannon Entropy value is present or the critical point changing the trend of Shannon Entropy can be considered as the optimum level. Among different wavelet functions, higher entropy value can be explained as more underlying information are recovered and contained in the approximation image. Thus, we look for the wavelet function which provides the maximum Shannon Entropy value at its optimal decomposition level.

3. Clustering pixel intensity values

Clustering analysis is a statistical method of partitioning a set of observations into several subsets which can be called clusters. The components in the same subset have a similar property to some extent (Jand et al., 1997). This feature in one subset is different from those in the other clusters so that clusters can be distinguished. The way to determine the similarity among components is based on a distance measure. A common used distance function for clustering analysis is the Euclidean distance. Clustering methods can be classified into three categories: hierarchical clustering, partitional clustering and spectral clustering. Fuzzy C-means Clustering belongs to the category of partitional clustering.

3.1 Fuzzy C-Mean Clustering

Fuzzy C-means Clustering (FCM) assigns each observation partly into a cluster (Bezdek J.C. 1981). Since data points can

always be considered in one cluster and also in another one in practical situations, the concept of fuzzy theory is applied in clustering method. Rather than belonging completely to one cluster, every observation has a degree of becoming a member of that cluster. In this way, all partitions are connected to each other. Thus FCM has special advantages over conventional clustering methods. For all the c clusters, the sum of the degree or the membership of each point should be 1.

$$\sum_{i=1}^{c} u_{ik} = 1, \text{for all the } c \text{ clusters}$$
$$0 \leq u_{ik} \leq 1$$
$$0 < \sum_{k=1}^{n} u_{ik} < n \qquad (6)$$

Where u_{ik} is interpreted as the degree of point k in the i-th cluster. The total number of input points and clusters are n and c respectively. u_{ik} satisfies the condition that its value is between 0 and 1. When u_{ik} equals 1, it means point i belongs to the i-th cluster completely; otherwise it is not the member of the i-th cluster at all if the value of u_{ik} is 0.

The degree u_{ik} itself can be calculated as the inverse of the distance measure between the point x_k and its corresponding cluster centre. The normalized and fuzzyfied form is used more widely. Introducing the weighting exponent m

$$u_{ik} = \frac{1}{\sum_{j}^{c} (\frac{d_{ik}}{d_{jk}})^{2/(m-1)}}$$
$$where\ d_{ik} = |x_k - v_i|;\ d_{jk} = |x_k - v_j| \qquad (7)$$

The cluster centre v_i is nothing but the average of all the observations in i-th cluster:

$$v_i = \frac{\sum_{k=1}^{n} u_{ik}^m x_k}{\sum_{k=1}^{n} u_{ik}^m} \qquad (8)$$

Similarly, v_j denotes the mean in j-th cluster. To divide observations into desired c clusters, FCM algorithm minimizes an objective function consisting of summation of weighted membership and squared error of the distance to the cluster centre through an iterative process.

$$J_{FCM} = \sum_{k=1}^{n} \sum_{i=1}^{c} u_{ik}^m d_{ik}^2 \qquad (9)$$

3.2 Fuzzy Range Clustering

Fuzzy Range Clustering (FRC) mainly investigates the differences in membership values of clusters generated from pixel intensities trough FCM. Supposing only two clusters are created and Mo_i and Mb_i are the membership values for point i in one fuzzy cluster and the other respectively. The fuzzy range for both clusters (R_i) is formulated as:

$$R_i = Mo_i - Mb_i, \text{for all the point } i \qquad (10)$$

R_i is a new and typical feature of touching areas besides traditional features such as gradient, standard deviation, etc.. From the standpoint of fuzzy clustering theory, the pixel intensities of touching areas have a similar degree of belonging to both clusters. It may be noted that the advantage of FRC over traditional features is that only the pixel intensities of interest is involved and is independent of the size of the neighborhood (Yang, Y. 2009).

4. Case Study

Particle images always contain touching and overlapping regions, making segmentation important and necessary. In this case study, the proposed separation technique combing wavelet transform and FCM algorithm is applied to particle image analysis to identify and separate objects and the result are compared with conventional segmentation approaches.

4.1 Imaging setup used in the present study

A laboratory scale software/hardware framework for capturing particle images for this case study was setup. In order to get images that can fairly represent samples of a real life particulate system, the experimental setting includes a system with a flow cell and pump, through which particles are continuously circulated, an illumination system for lighting up the imaged region of the flow cell, an optical zoom system for providing magnification and a digital video camera for continuous image capture. Figure 1 illustrates the schematic diagram of the experimental set up. The camera used is a CMOS chip based video camera (BASLER make, model A620f) with a resolution of 1024 X 1280 pixels and is connected to the computer using a IEEE 1394 cable. The particles were circulated with water using a pump (Watson Marlow UK). An optical zoom system (Thales Optem zoom125C) with maximum magnification of 150X was fitted to the camera lens. A software framework developed in MATLAB enables the configuration of image acquisition parameters. The particles used are Poly Vinyl Chloride (PVC) particles of refractive index of about 1.5.

4.2 Application

The original grey particle image in a JPG format was imported into MATLAB for processing. To simplify the calculation, it was cropped into an image possessing 1024*1024 pixels shown in Figure 2a. Visual observation reveals a total of 15 particles in this image, all of which are sequentially labelled from 1 to 15. Manual partition and measurements were determined in the software of ImageJ (V1.42q, NIH, USA). In the previous work, a nonlinear filter namely order statistics filters was chosen to process the image (Korath et al., 2008). In our research we are using wavelet for this purpose.
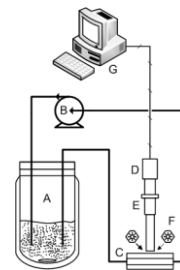

Figure 1: Schematic diagram of the image acquisition setup: (A) Vessel with particle suspension, (B) Circulating pump, (C) Optical flow cell, (D) Camera, (E) Zoom system, (F) Illumination, (G) Computer.
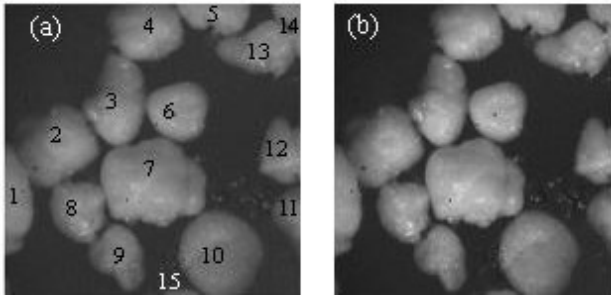
Figure 2: (a) Original particle image and (b) First approximation image of (a).

To obtain the optimal solution, four common wavelet families and six decomposition levels for each wavelet function were considered. The entropy values of the approximation images are listed in Table 1. In each data column, the first minimum number was highlighted in bold. Some of them reached the minimum at the first decomposition level. Implementation of the wavelet transform only once by wavelet functions such as db3, coif1, and coif3 would be enough to remove noise and high frequency components and obtain smooth surfaces of the particles. On the other hand, for wavelet functions Haar, db6, sym4, and sym8, their spatial and frequency characteristics cannot remove surface noise in the first approximation so that more decomposition steps are needed to reach the lowest entropy value. Once this first minimum entropy is reached, on further decomposition, the artifacts from the wavelet function will be added to the particle surface which will make the surface irregular and correspondingly increase the Shannon Entropy. The decrease of entropy value after this increase in further decomposition level is due to the relative smooth surface shaped as a result of the removal of irregular parts. Taking this into consideration, the second or the third minimum point is meaningless since plenty of real information has been eliminated. By comparing those minimum values among different wavelet functions, the greatest was found to be 2.2661. This indicates that db3 can retain more information than the other wavelet functions. The approximation image generated through wavelet transform by wavelet function of db3 at the first decomposition level was chosen for further processing and it was shown in Figure 2b.

Table 1: Minimum Shannon Entropy (1.000e+004) for different wavelet functions and decomposition level

	Haar	db3	db6	sym4	sym8	coif1	coif3
1st	1.9968	**2.2661**	2.2644	2.348	2.1095	**2.1579**	**2.0987**
2nd	1.9696	2.2736	2.2558	**1.9792**	2.0698	2.2484	2.2659
3rd	1.944	2.2401	2.1278	2.3523	**2.065**	1.9628	1.9866
4th	1.9176	2.2152	2.0458	2.4132	2.2069	2.2373	2.2663
5th	**1.9171**	2.2372	**2.0195**	2.4357	2.2773	2.3616	2.2801
6th	1.9865	2.4014	2.0196	2.3321	2.1604	2.3121	2.1435

The first approximation image was then simply divided into objects and backgrounds by thresholding which is a segmentation method based on a threshold value. The Otsu's method of selecting a threshold from grey level histograms

was chosen in this work. Objects were formed where the pixel intensities are greater than the threshold value and the background is assigned where they are less than the threshold value. The binary image with labels on each particle shown in Figure 3 shapes the objects whose values are 1 and the rest are the background with the value of 0. Some particles are connected to each other in the binary image. They were considered as a single object resulting in wrong particle sizing. The number of particles and particle size calculated from this binary image is used as a comparison to the partition result from the FCM approach.
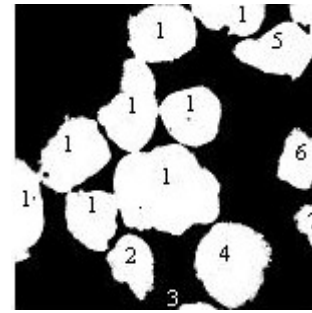

Figure 3: Thresholded image of Figure 2b.

When partitioning the first approximation image into two clusters, representing the objects and the background, two membership images are generated as shown in Figures 4a and 4b. Figure 4c describes the membership value versus pixel intensity. The weighting exponent m, the maximum number of iterations and objective error as the FCM parameters used in this paper are 2, 500 and 10^{-5} respectively. The influence of iterations number has been investigated as well and it is found that the same result can be obtained if the iterations number is chosen between 500 and 1000.
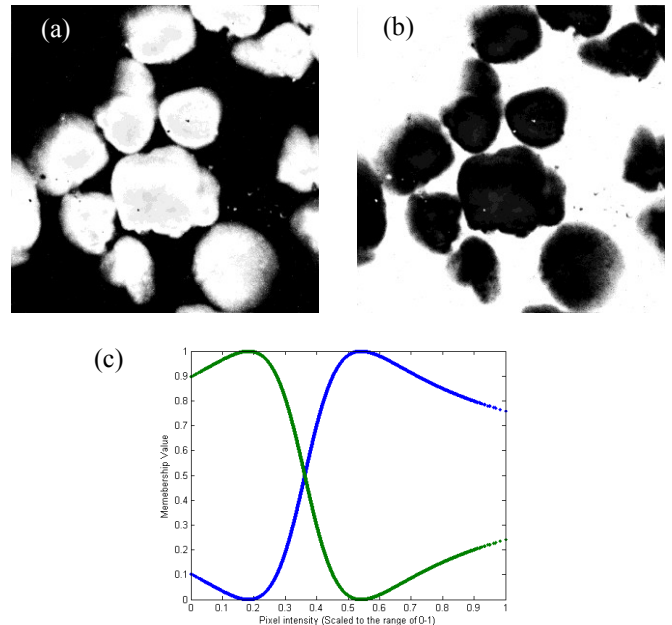

Figure 4: (a) High membership of object cluster and (b) High membership of background cluster; (c) Cluster membership value versus pixel intensity.

On closer examination of the membership values of the touching regions in both images, it can be observed that they

142

are similar. This may be due to the fact that their pixel intensity values are between those in the two clusters. The touching region image was obtained by subtracting the two membership images using FRC.

To achieve the separation, the touching region image was transformed into a binary image and then removed from the above mentioned thresholded image. After performing proper morphological operations deleting holes and spurs, the final results shown in Figure 5a were obtained. The labels of separated particles are printed on the image. Figure 5b shows the separated particle image using median filter.
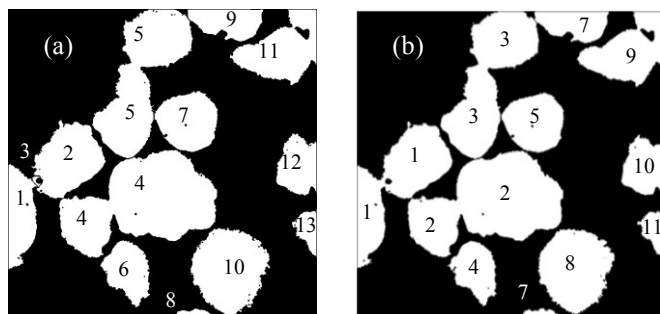

Figure 5: (a) Separated particle image (b) Partition results using median filter

4.3 Equivalent Diameter and PSD

The particle number, particle equivalent diameter, and particle size distribution (PSD) are considered to illustrate the separation efficiency. The comparison involves Figure 5a (resulting from Wavelet-FCM approach), Figure 2a (the manual processed image) and Figure 3 (thresholded image). The comparison of the Wavelet-MFC method with the median filter approach with respect to segmentation level (Figure 5b) is also discussed as well. The thresholded image has 7 particles and the separated image (Figure 5a) contains 13 particles. The extra number was coming from separation of the touched objects which were considered as one single connected component. However, the approximation image was not over partitioned since there are actually 15 particles by visual examination. Although some particles are separated, particle 4, 5, and 11 are connected in Figure 5a.

The equivalent diameter, defined as the diameter of a circle that has the same area of that object, is used to describe the size of the particles. It is counted as the number of pixels. Their values in thresholded image, separated one using Wavelet-MFC approach, and manual processed image are listed in Table 2. Particles in Figure 2a were identified manually as circles or ellipses. The same particle was chosen from the above mentioned three images to compare their sizes. For example, particle 2 in thresholded image, particle 6 in separated image, and particle 9 in the original image are selected. The diameter found in the separated image is smaller compared with that from the theresholded image while both are greater than manual measurements. The differences between thresholded image and separated image are generated from the boundary region. The particles shrink after segmentation because of the missing parts in edges which are considered as components of touching regions and are deleted. The differences with manual measurements are

caused by non-accuracy of modelling particle with ellipses. PSD provides direct information of the distribution of the equivalent diameters in a certain range and their normalized frequencies. The histogram of equivalent diameters and their fitting curves through Weibull density probability function are used to describe the PSD. From Figures 6a and 6b, we can conclude that by breaking down the touched objects, the mean size decreases and the size distribution became sharper; with high frequency of appearance of the particles with similar size and less dispersion of the large diameter values. This brings the PSD generated via the Wavelet-MFC approach closer to the reference PSD obtained by manual processing (Figure 6c) in which a large proportion of particles have equivalent diameters in the range of 50 to 250.

It is also interesting to compare the partition results using the wavelet transform instead of median filter as reported in Korath et al., (2008). Particle 1 in Figure 5b cannot be separated but it was divided in Figure 5a. So the introduction of the wavelet transform improves the segmentation of particle images.

Table 2: Particle equivalent diameter

Particle label	Thresholded image	Wavelet-MFC approach	Manual processed image
1	630.2500	176.3487	126.5848
2	**171.3837**	227.9044	175.9982
3	55.8177	21.7926	169.0084
4	262.0052	375.4876	153.8821
5	230.0344	310.8905	106.6184
6	164.4029	**169.3584**	139.9372
7	99.2525	53.2734	216.7311
8		199.0270	135.0288
9		156.0879	**131.6775**
10		260.4186	196.3898
11		224.7657	85.9274
12		161.6972	120.8894
13		95.7129	134.1396
14			82.8725
15			41.7805

5. Architecture of the image-based monitoring framework

For reliable performance, a monitoring system must include components of acquisition, storage and processing of the data as well as display and storage of the information content of the data. The hardware, software and associated communication interfaces have to suitably constitute to satisfy the requirements in terms of speed, scale and interoperability with other systems in an industrial environment. In the case of image-based monitoring, the acquired images form the primary input data and they are stored in a database. Information of this data is to be extracted and made available in a form required by the process monitoring methodologies. The input data repository should be available for different schemes of information extraction and have to reach to the performance requirements with respect to storage and retrieval. The data base of information extracted from images, such as features of objects, also has to meet similar criteria of storage and

143

accessibility by multiple methodologies. The typical architecture is depicted in Figure 7. The image processing algorithms constitutes the main software module of the proposed system. The procedures of processing images include pre-processing, segmentation and feature extraction. The pre-processing methods have to be chosen depending on the kind of degradation the images in a particular system and environments are exhibiting. A Graphical User Interface (GUI) provides the human interaction with the system for visualization, conducting manual analysis and system configuration/management. A sample GUI for the current study is presented in Figure 8. The interface includes configuring the image acquisition setup, selecting the pre-processing and segmentation methods, viewing the images when they are analyzed, visualization of feature data in charts or trends curves, and displaying the comparison between before and after segmentation. The image size, de-noising methods of wavelet transform and median filter, clustering basis of fuzzy range and traditional features can be selected through the GUI. Also, the processed image for each stage, size distribution graph, the particle numbers of thresholded image and separated image, and the adopted wavelet function and decomposition level are shown.
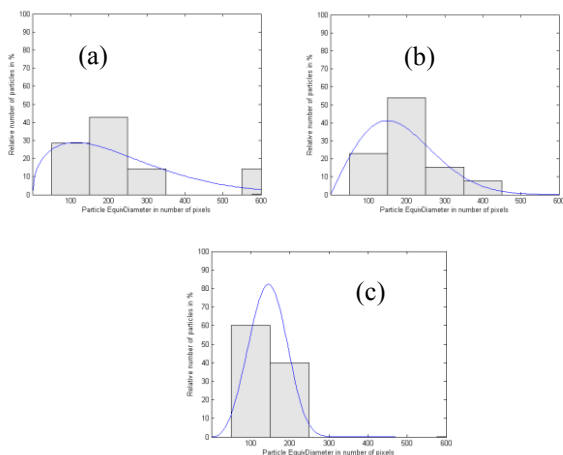

Figure 6: Particle size distribution of (a) before and (b) after segmentation using Wavelet-MFC approach; (c) manual measurement.

6. Conclusions

An image segmentation approach of combing wavelet transform and FCM was proposed and applied in the case study of particle image segmentation to testify its efficiency. This method could successfully identify 13 out of a total of 15 objects and it was found to be superior to previous approaches. The image was not over partitioned and the particle equivalent diameters and size distribution in the separated image were more meaningful.

References

Addison P.S. (2002), *The illustrated wavelet transform handbook*, Introduction theory and application in science, engineering, medical and finance, Institute of Physics Publishing, Bristal and Philadephia.

Cufi X., Munoz X., Freixenet J., Marti J. (2002), A review of image segmentation techniques integrating region and boundary information, *Advances In Imaging And Electron Physics*, **120**, 1-39.

Bezdek J.C. (1981), *Pattern Recognition with Fuzzy Objective Function Algorithms,* Plenum Press, New York.

Fu K.S. and Mui J.K. (1981), A survey on image segmentation, *Pattern Recognition*, **13**, 3-16.

Jand J.S.R., Sun C.T., Mizutani E. (1997), *Neuro-Fuzzy and soft computing,* P423-425, Prentice Hall Inc. A. Pearson Education Company, New Jersey.

Korath J.M., Abbas A., Romagnoli J.A. (2008), A clustering approach for the separation of touching edges in particle images, *Particle & Particle Systems Characterization,* **25**(2), 142-153.

Pal N.R. and Pal S.K. (1993), A review of image segmentation techniques, *Pattern Recognition*, **26**, 1277-1294.

Sun W., Mukherjee R., Stroeve P., Palazoglu A., Romagnoli J.A. (2008), A multi-resolution approach for line-edge roughness detection, *Microelectronic Engineering,* **86**(3), 340-351.

Sun W., Romagnoli J.A., Tringe J.W. Letant S.E., Stroeve P., Palazoglu A. (2009), Line edge detection and characterization in SEM images using wavelets, *IEEE Transactions on Semiconductor Manufacturing*, **22**(1), 180-187.

Yang Y. (2009), Image segmentation based on fuzzy clustering with neighbourhood information, *Optica Applicata*, **39**(1), 135-147
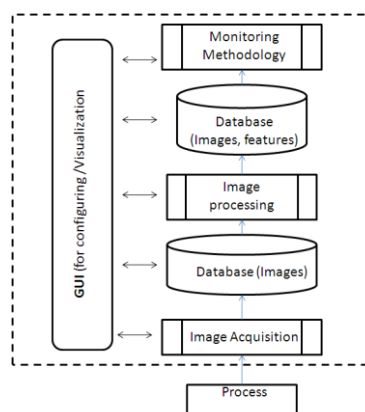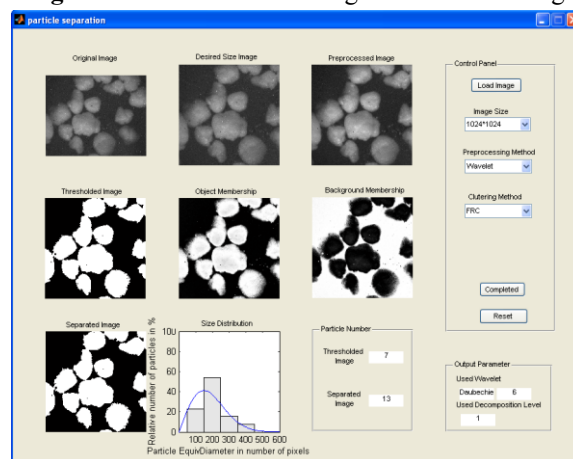
Figure 7: Framework for image-based monitoring

Figure 8: GUI for Multi-resolution Fuzzy Clustering method